

## Enhanced biological production in the southeastern Arabian Sea during spring intermonsoon

C.M. Laluraj<sup>a\*</sup>, K.K. Balachandran<sup>b</sup> and P. Sabu<sup>a</sup>

<sup>a</sup>National Centre for Antarctic and Ocean Research, Headland Sada, Goa, India;

<sup>b</sup>National Institute of Oceanography, Council of Scientific and Industrial Research (CSIR), Regional Centre, Kochi, India

(Received 20 December 2011; final version received 2 August 2012)

Hydrographic observations in the southeastern Arabian Sea (SEAS) have identified a warm ( $>30^{\circ}\text{C}$ ) and stratified water mass (stability  $>5 \times 10^{-5} \text{ m}^{-1}$ ) along the near shore area between  $10^{\circ}\text{N}$  and  $15^{\circ}\text{N}$  during spring intermonsoon. This water mass was relatively low saline (34.2) and nitrate-rich ( $0.5 \mu\text{M}$ ), favoring moderate primary production ( $6.7 \text{ mg C m}^{-3} \text{ d}^{-1}$ ). Since the mixing of the Arabian Sea and the Bay of Bengal waters is an important process during this period, the enhanced primary production in the SEAS is attributed to the entrainment of unconsumed nitrate left over during the previous season from the northern Arabian Sea. The season was further characterized by the presence of a deep chlorophyll *a* maximum ( $0.5 \text{ mg} \cdot \text{m}^{-3}$ ) in the outer shelf below ( $>50 \text{ m}$ ) the subducted Arabian Sea High Saline Waters, which was photosynthetically less active ( $<1.5 \text{ mg C m}^{-3} \text{ d}^{-1}$ ) due to light limitation.

**Keywords:** southeastern Arabian Sea; salinity; stratification; warm pool; phytoplankton; primary production; algal blooms; spring inter monsoon

### Introduction

The Arabian Sea and the Bay of Bengal are two tropical basins of the North Indian Ocean separated by the Indian subcontinent. The oceanographic features of these basins are principally controlled by the reversing monsoonal winds [1]. The high salinity (35–37) in the Arabian Sea is caused by an excess evaporation over precipitation [2], whereas the persistently low salinity in the Bay of Bengal is caused by an excess precipitation (river discharge) over evaporation [3]. The winds over the Indian Ocean undergo an annual reversal, as they are southwesterly during SW Monsoon (May–September) and northeasterly during NE Monsoon (November–January). The spring intermonsoon (SIM) is a transition period between winter and summer monsoons when the winds are generally weak but the high solar irradiance warms up the surface layers [4]. Concurrently, the intrusion of low salinity Bay of Bengal waters influences the hydrography of the South Eastern Arabian Sea (SEAS) by establishing surface stratification [5–7]. The warming of the SEAS (SST;  $>28^{\circ}\text{C}$ ) during February–April, known as Arabian Sea Mini Warm Pool (ASMWP), is believed to be an important condition for the onset of the south west

---

\*Corresponding author. Email: lalucm@ncaor.org

monsoon in India [7,8]. The formation of warm pool and subsequent stratification is found to enhance biological production that varies seasonally and inter-annually [9–12]. However, the responses of such secondary heating processes on the onset of southwest monsoon have so far been studied mostly from a physical oceanographic context. In this paper, we examine the environmental characteristics of the SEAS following the formation of a mini warm pool during an early SIM season and its impact on phytoplankton production.

### Material and methods

The hydrographic data from the SEAS (8°–15°N and 69°–77°E) were collected during a cruise (SS223) in the Fisheries and Oceanography Research Vessel *Sagar Sampada* during March–April 2004 under the programme *Environment and Productivity Patterns in the Indian Exclusive Economic Zone* funded by Ministry of Earth Sciences, New Delhi (Figure 1). Surface meteorological parameters were recorded on a shipboard Automatic Weather Station (AWS). SST was measured using a bucket thermometer (accuracy  $\pm 0.10^\circ\text{C}$ ). Vertical profiles of temperature and salinity data were collected using a Conductivity-Temperature-Depth rosette profiler (CTD, Seabird Electronics, temperature accuracy  $\pm 0.001^\circ\text{C}$ , salinity accuracy  $\pm 0.0001$ ) equipped with 1.8 L Niskin water samplers. CTD salinity values were calibrated with on-deck analysis of discrete water samples using a Guideline 8400 AUTOSAL (Ocean Scientific International, Pertersfield, UK). Water samples collected from standard depths from all stations were analysed for nitrate and silicate using an onboard Auto Analyzer (Skalar Analytical, Netherlands). Primary production (PP) was measured by the radiocarbon ( $^{14}\text{C}$ ) method [13,14]. Water samples collected from seven depths (surface, 10, 20, 50, 75, 100 and 120 m) using Go-Flo samplers were transferred to 300 ml polycarbonate bottles (Nalgene, Germany). Each bottle was inoculated with 1 ml of  $\text{NaH}^{14}\text{CO}_3$  ( $5 \mu\text{Ci ml}^{-1}$ , Board of Radioisotope Technology, Department of Atomic Energy, India) and the bottles were suspended at the approximate depths of sampling using a polypropylene line attached to a buoy for incubation. Three light bottles and one dark bottle were used at each depth. The incubation lasted from approx 1 h before sunrise to 30 min after sunset ( $\sim 13$  hrs) after which, the samples were retrieved and filtered using GF/F filters ( $0.7 \mu\text{m}$ ) under low vacuum ( $< 5$  psi). The filters were exposed to concentrated HCl fumes to remove excess inorganic carbon and transferred to scintillation vials for subsequent estimation. Liquid scintillation cocktail (Sisco Research Laboratory, Mumbai) was added to the vials and after about a day, they were counted in a scintillation counter (Wallace 1409 DSA, Perkin–Elmer, USA). The disintegration per minute (DPM) was converted into daily production rates ( $\text{mg C m}^{-3} \text{d}^{-1}$ ) by taking into account the initial activity and adsorption of  $^{14}\text{C}$  by particles in the bottles [15]. Dark bottle production was subtracted from the light bottle to correct for non-photoautotrophic carbon fixing. Samples for chlorophyll analysis were also taken from the same casts as that of primary productivity (Figure 1). One litre of seawater was collected from each depth and passed through GF/F filters ( $0.7 \mu\text{m}$ ). Chlorophyll *a* estimation was carried out using a spectrophotometer (UV-1650PC Shimadzu) after extraction with 10 ml 90% acetone in the dark [16]. The chlorophyll *a* (Chl *a*) was calculated using appropriate calibration factor. Water column primary production ( $\text{mg C m}^{-2} \text{d}^{-1}$ ) and Chl *a* ( $\text{mg m}^{-2}$ ) were calculated by integrating the respective values over depth. Stability of the water column was determined for each

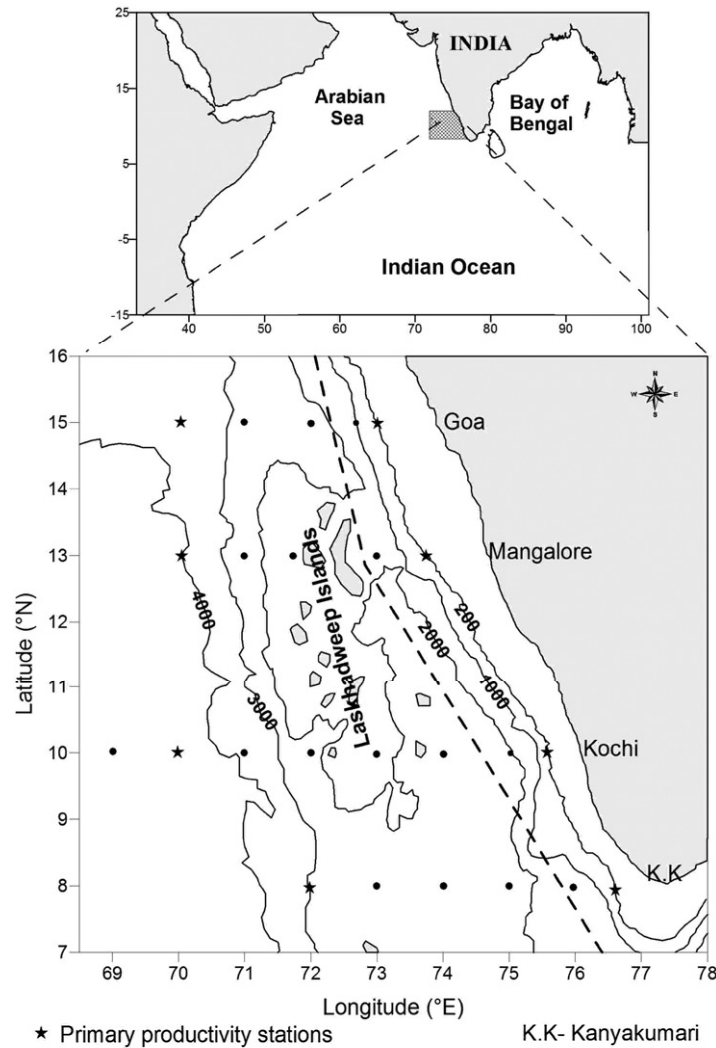


Figure 1. Station locations in the South Eastern Arabian Sea. Depths are given in meters. Coastal and offshore stations are separated by dotted line.

1 m-pressure slab up to 100 m. Mixed layer depth (MLD) was defined here as the depth at which temperature dropped by 1°C from the sea surface. Heat content of the surface layer (50 m) within the photic depth (~55 m) was calculated from

$$H = \rho C_p \left[ \int_0^z T \cdot dz \right]$$

where,  $H$  is the heat content ( $J m^{-2}$ ),  $\rho$  is the density of seawater ( $1024.5 kg m^{-3}$ ),  $C_p$  is the specific heat ( $4000 J kg^{-1} °C^{-1}$ ) at constant pressure and  $T$  is the depth averaged temperature obtained from the CTD (surface to 50 m). The value of  $\rho C_p$  is taken as constant ( $0.409 \times 10^7 J m^{-3} °C^{-1}$ ) [17].

### Results and discussion

The meteorological conditions over the SEAS were generally characteristic of the SIM season (clear sky, high solar insolation and weak winds of  $\sim 4$  m/s). Even though the air temperature ( $29.2$ – $30.4^\circ\text{C}$ ) generally varied diurnally, the coastal waters were warmer ( $> 30^\circ\text{C}$ ) with shallow mixed layer (MLD  $17$ – $35$  m, Figures 2a and 3a). The warm waters were spread around  $100$ ,  $400$  and  $200$  km along  $15^\circ\text{N}$ ,  $13^\circ\text{N}$  and  $10^\circ\text{N}$  respectively (Figure 4), with a maximum thickness of  $25$  m at  $13^\circ\text{N}$ . A low saline water mass ( $< 34.4$ ) was found juxtaposed over the warm ( $> 30.2^\circ\text{C}$ ) surface layer extending down up to  $50$  m along the shelf at  $8^\circ\text{N}$  (Figure 2a, b). The mixing of low saline (Figure 5) and high saline waters ( $> 35.4$ ) have established stratification in the surface waters between  $10$ – $15^\circ\text{N}$ , which

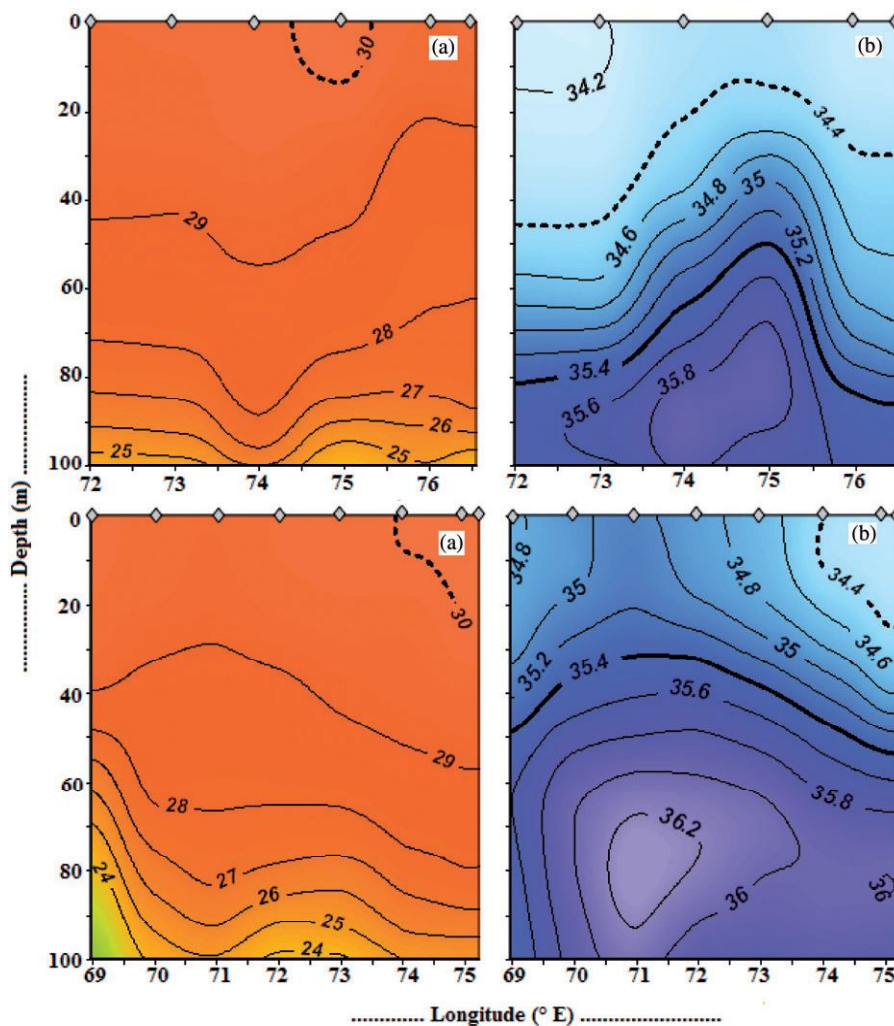


Figure 2. Vertical distribution of temperature (a) and salinity (b) along  $8^\circ\text{N}$  (top panel) and along  $10^\circ\text{N}$  (bottom panel). The  $35.4$  isohaline is represented by thick line, whereas  $30^\circ\text{C}$  isotherm and  $34.4$  isohaline are represented by broken lines. Diamond symbol represents station locations.

eventually gained a heat content of  $101.1 \text{ W m}^{-2}$  [18]. The nitrate content of this water mass also increased from  $0.5 \mu\text{M}$  along  $10^\circ\text{N}$  to  $1.0 \mu\text{M}$  along  $13^\circ\text{N}$  (Figures 6a and 7d). However, the silicate rich ( $1 \mu\text{M}$ ) waters entering the SEAS from the Bay of Bengal was found spread up to  $70^\circ\text{E}$  along  $8^\circ\text{N}$ , eastward up to  $73^\circ\text{E}$  along  $10^\circ\text{N}$  and northward up to  $15^\circ\text{N}$  at 50 m (Figures 6b and 7e).

The circulation in the SEAS is generally influenced by the Winter Monsoon Current (WMC) and the Western India Counter Current (WICC) [19]. Despite the fact that the circulation in the AS reverses annually from southerly (April–September) to northerly (November–February), their influence on the northern AS is obscured due to intense winter cooling. The intrusion of Bay of Bengal waters into the Arabian Sea starts from

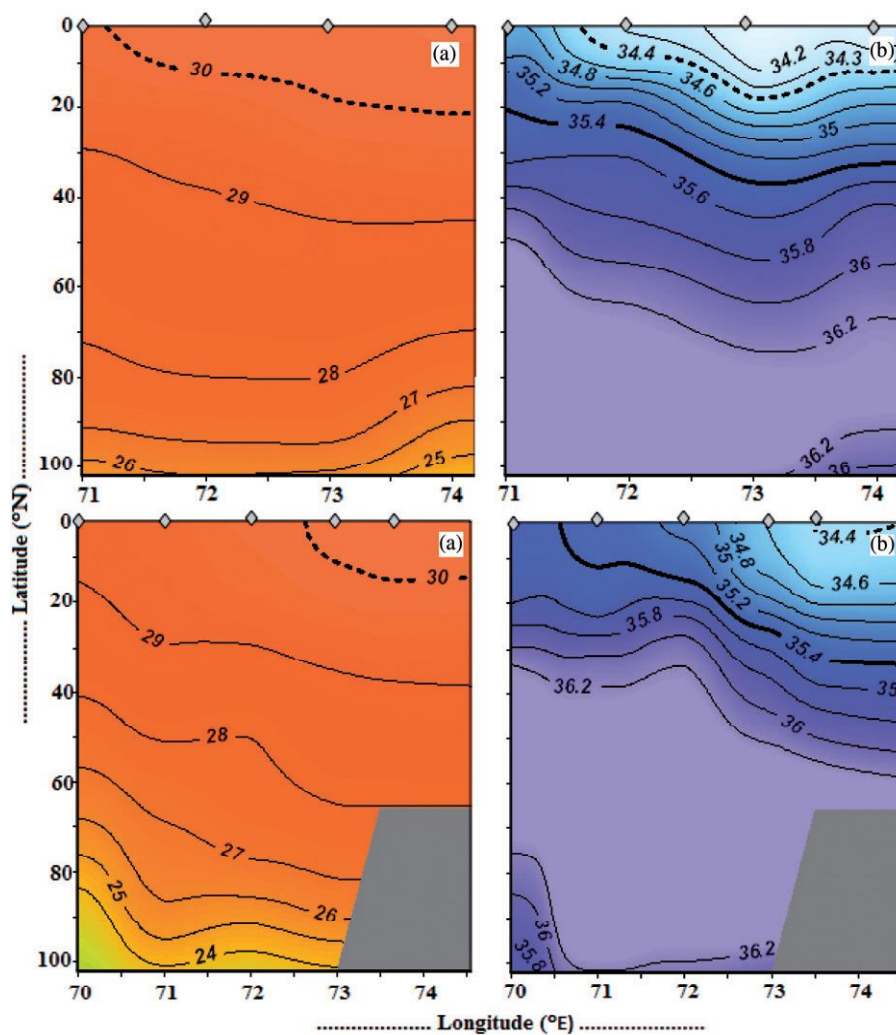


Figure 3. Vertical distribution of temperature (a) and salinity (b) along  $13^\circ\text{N}$  (top panel) and  $15^\circ\text{N}$  (bottom panel). The  $30^\circ\text{C}$  isotherm and  $35.4$  isohaline are represented by thick lines and the  $34.4$  isohaline by broken lines. Diamond symbol represents station locations.

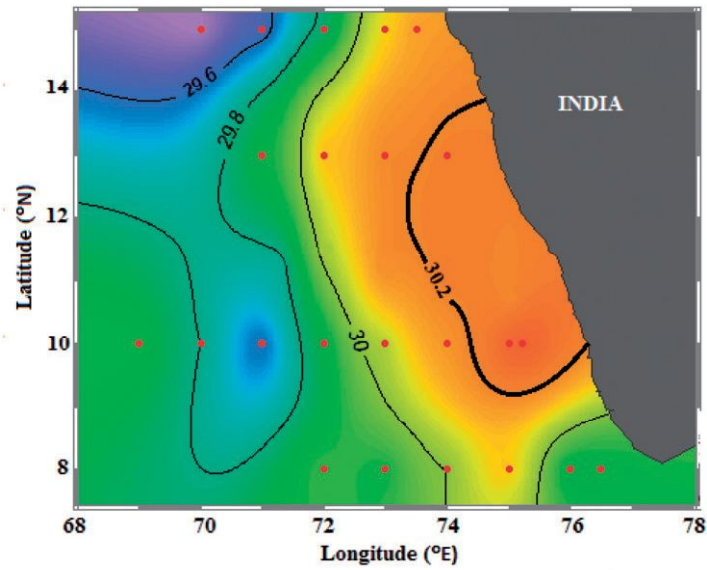


Figure 4. Distribution of sea surface temperature in the SEAS. The warm pool ( $>30^{\circ}\text{C}$ ) is marked by thick line.

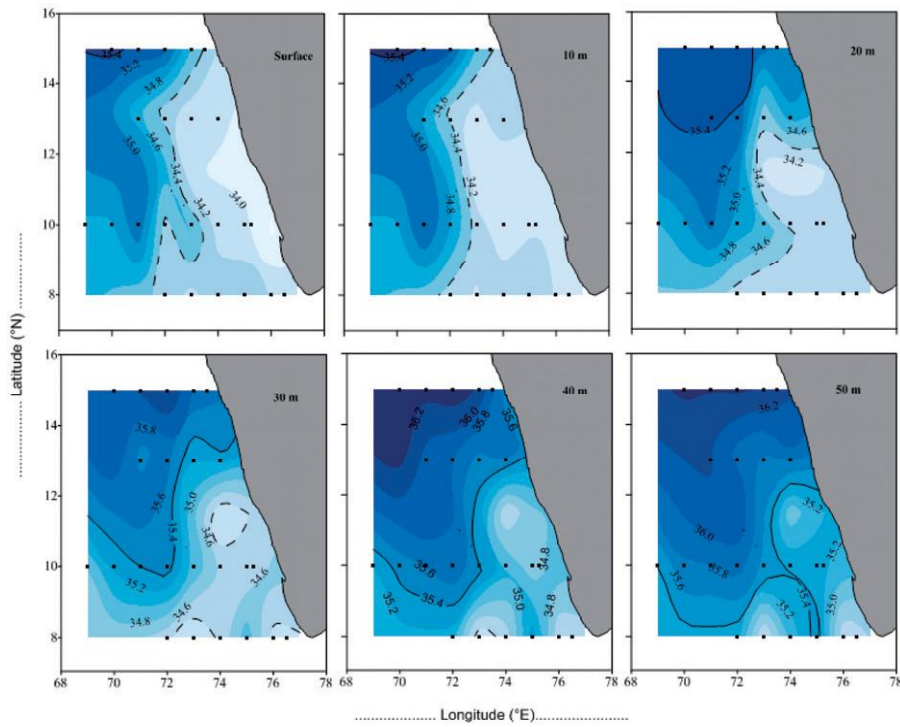


Figure 5. Distribution of salinity at surface, 10, 20, 30, 40 and 50 m depths showing the advection of ASHSW into the SEAS (solid line represents the 35.4 salinity and broken line represents 34.4).

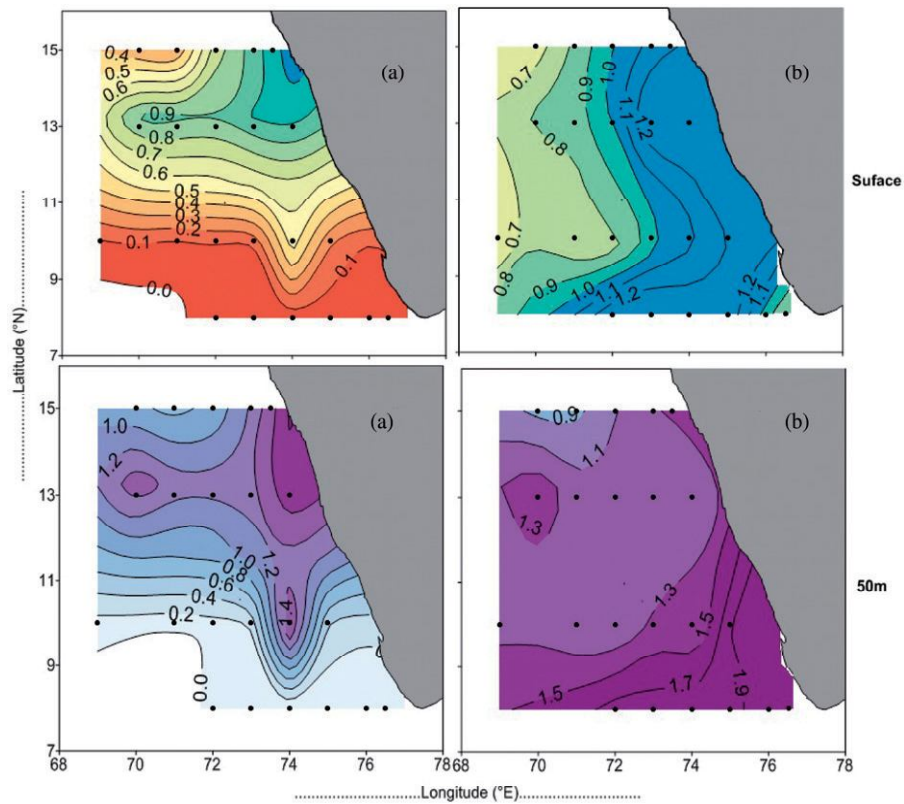


Figure 6. Distribution of nitrate (a) and silicate (b) along the surface and 50 m (concentrations are expressed in  $\mu\text{M}$ ).

early December, when the WMC feeds into the poleward flowing WICC [1,20]. The strong cross-shelf variation in salinity is evident from a branch of WMC deflecting westward off  $8^\circ\text{N}$  spreading the low salinity waters between  $76.3^\circ\text{E}$  and  $72^\circ\text{E}$ , whereas its northerly component enters Lakshadweep Sea and flows poleward up to  $15^\circ\text{N}$  in a narrow stretch between  $75^\circ\text{E}$  and  $76^\circ\text{E}$ . While the WICC reverses its flow in February along southwest India, it is still poleward along the rest of the coast (north of  $15^\circ\text{N}$ ) until May [6,21]. The present observation being a transition period (March), the currents in the SEAS are either weak or directionless. As the low-salinity Bay of Bengal waters glide over the Arabian Sea High Saline Waters (ASHSW), they undergo mixing under the influence of small eddies [19]. The subduction of the northern Arabian Sea water mass is traceable from the dipping isohalines of salinity (35.4, Figures 5 and 7b). The stratification (Figure 7a, c) followed by the warming of the SEAS between  $10^\circ\text{N}$  and  $15^\circ\text{N}$  could be indications of the ASMWP (Figures 4 and 7a). Mixing of these different water masses (salinity 34.4) enriched in nitrate ( $1.0\ \mu\text{M}$ ) was found to support a fairly high phytoplankton growth (Figure 8a, b). It is likely that the nitrate enrichment in the SEAS is due to the entrainment of the northern Arabian Sea waters.

It is evident that between  $10^\circ\text{N}$  and  $15^\circ\text{N}$  in the SEAS, the surface chlorophyll *a* ( $0.51\ \text{mg}\ \text{m}^{-3}$ ) and surface PP ( $5.5\text{--}6.7\ \text{mg}\ \text{C}\ \text{m}^{-3}\ \text{d}^{-1}$ ) showed an increasing trend towards the coast (Figure 8a, b). The Central and Eastern Arabian Sea are generally found to

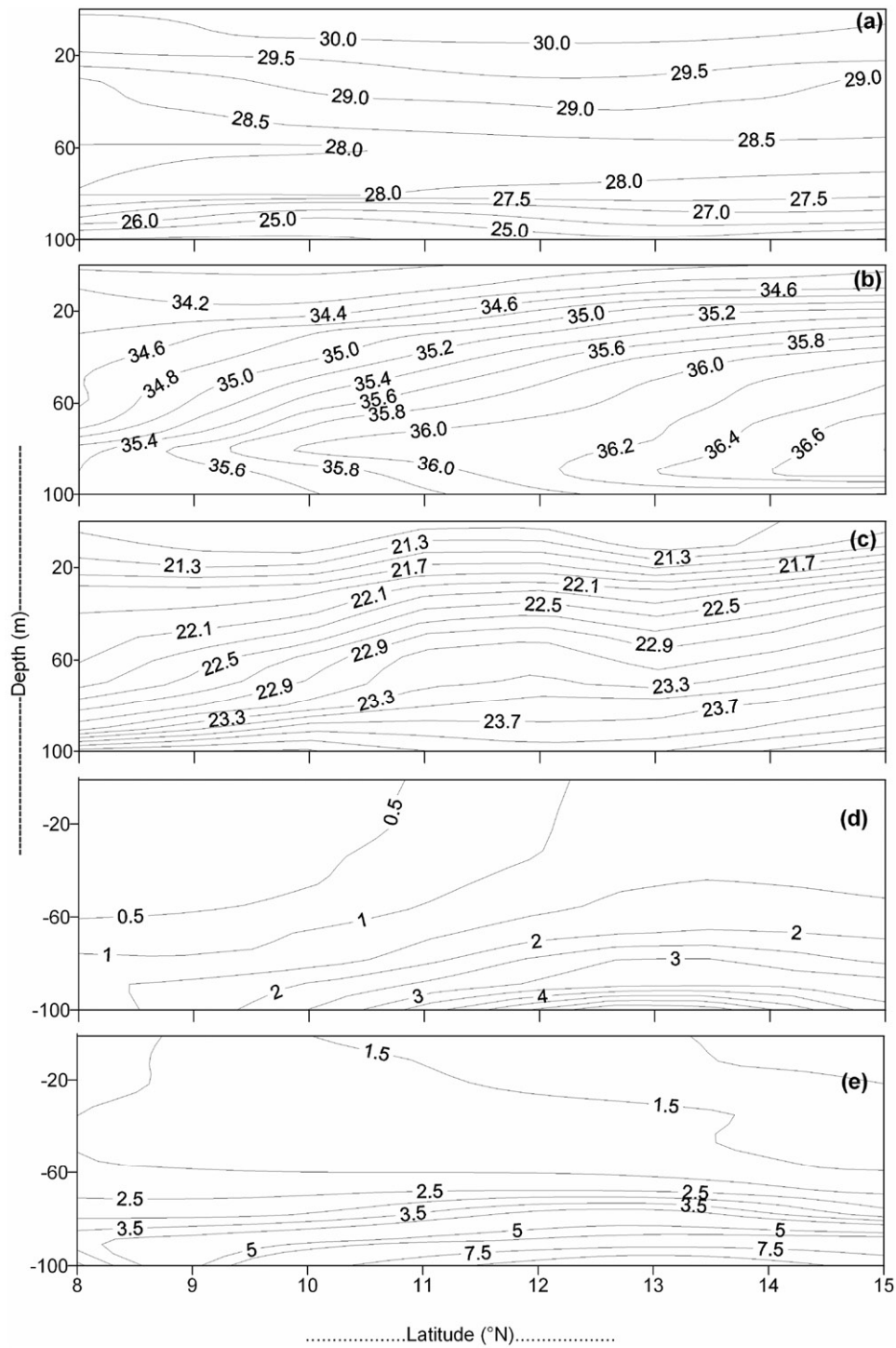


Figure 7. Latitudinal variation of (a) Temperature ( $^{\circ}\text{C}$ ), (b) Salinity, (c) Density ( $\text{kg m}^{-3}$ ), (d) Nitrate ( $\mu\text{M}$ ) and (e) Silicate ( $\mu\text{M}$ ) along the 200 m depth stations from all longitude.



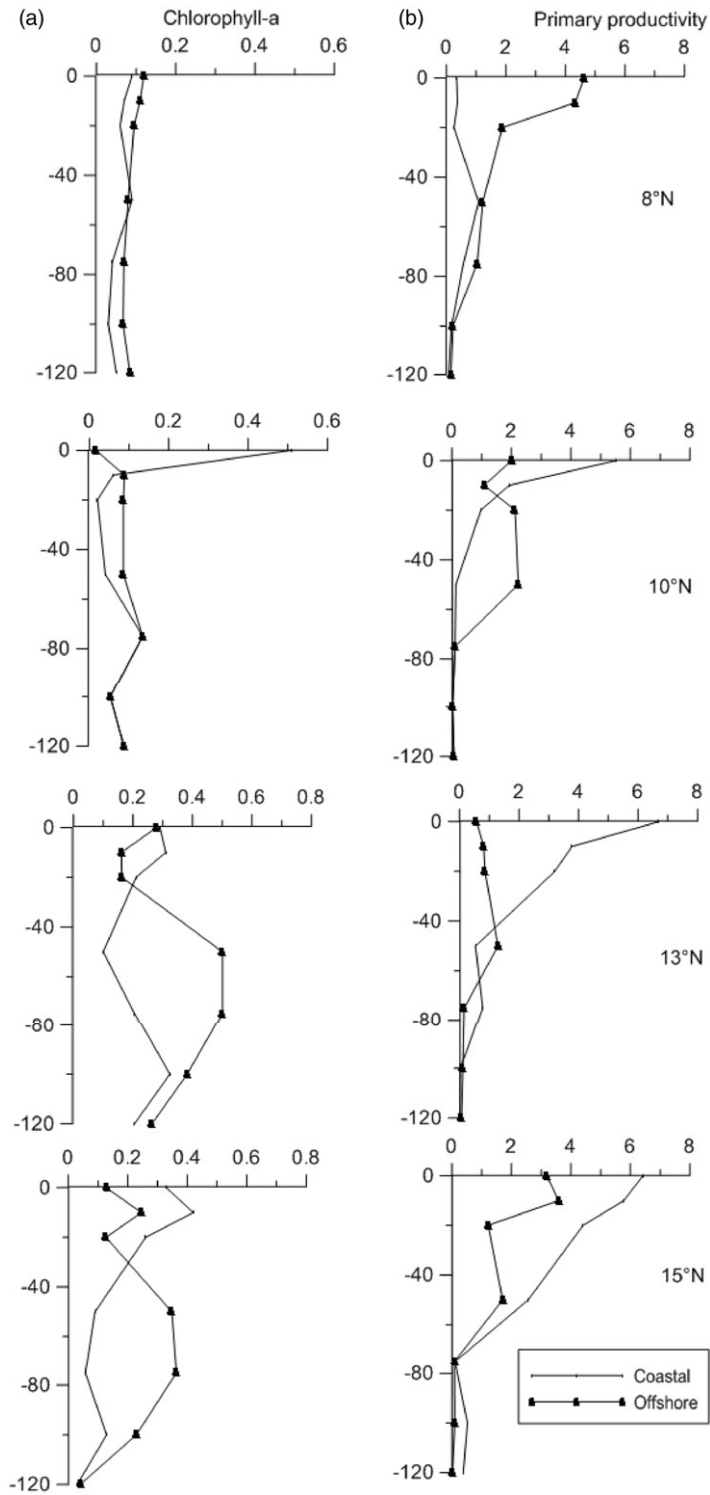


Figure 8. Vertical distribution of (a) Chlorophyll *a* (mg.m<sup>-3</sup>) and (b) PP (mgC.m<sup>-3</sup>.d<sup>-1</sup>) in the coastal and open ocean locations.

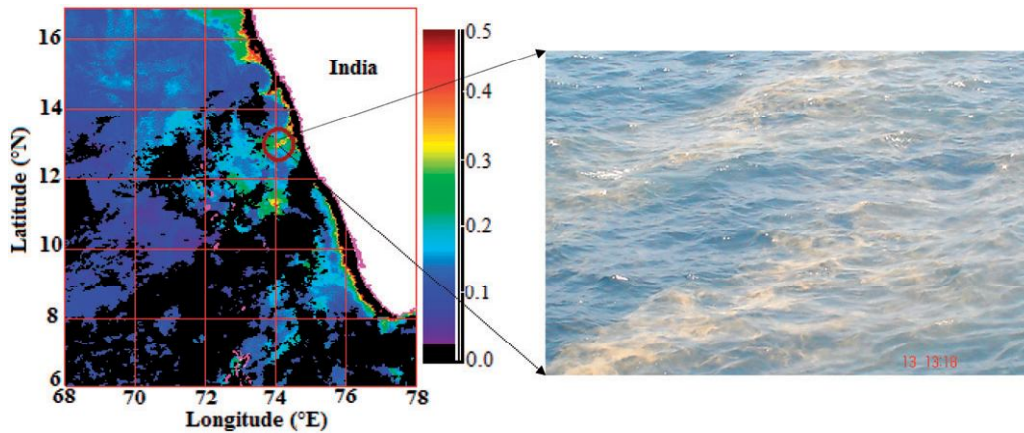


Figure 9. Aqua MODIS Chl  $a$  ( $\text{mg m}^{-3}$ ) concentration (6–13 April 2004) generated by NASA and phytoplankton bloom observed from site.

sustain low surface Chl  $a$  ( $0.4 \text{ mg m}^{-3}$ ) and primary productivity ( $2.6 \text{ mg C m}^{-3} \text{ d}^{-1}$ ) during this period [11]. Recently, Madhu et al. [22] observed high chlorophyll  $a$  biomass (av.  $0.81 \pm 0.80 \text{ mg m}^{-3}$ ) and primary production (av.  $29.5 \pm 23.6 \text{ mg C m}^{-3} \text{ d}^{-1}$ ) in northern Arabian Sea during early spring intermonsoon 2000.

Despite the formation of a mini warm pool and associated plankton growth, the SEAS (between  $13^\circ\text{N}$  and  $15^\circ\text{N}$ ) was also characterized by the presence of a Deep Chlorophyll Maximum (DCM;  $0.35\text{--}0.52 \text{ mg m}^{-3}$ ) between 40–80 m in the continental shelf, as reported previously [14,18]. The DCM along  $13^\circ\text{N}$  was dominated by diatoms such as *Rhizosolenia alata* spp. ( $380 \text{ ind.m}^{-3}$ ), *Chaetoceros* spp. ( $60 \text{ ind.m}^{-3}$ ) and *Thalassiosira* spp. ( $40 \text{ ind.m}^{-3}$ ), whereas that along  $15^\circ\text{N}$  was *Rhizosolenia alata* spp. ( $260 \text{ ind.m}^{-3}$ ), *Leptocylindrus* spp. ( $80 \text{ ind.m}^{-3}$ ) and *Thalassiosira* spp. ( $60 \text{ ind.m}^{-3}$ ). There was also the presence of some dinoflagellate (*Protoperidinium* spp.) in both locations ( $180$  and  $480 \text{ cells m}^{-3}$  respectively). Since the depth of the DCM and the depth of ASHSW (Figures 2, 3, 5 and 8) were more or less identical, it is likely that the development of DCM was favoured by the nitrate available in the subducted ASHSW (i.e. southwards moving WICC).

It would be quite significant to identify the source of nitrate leading to the phytoplankton blooms along  $13.5^\circ\text{N}$  and  $73.5^\circ\text{E}$  (Figure 9; observed on 13 April 2004). In order to explain the processes involved, the following observations from the Arabian Sea are summarized:

- (1) The low  $f$  ratios obtained from deck incubations at TN 43 of US JGOFS was attributed to phytoplankton's preference for  $\text{NH}_4^+$  over  $\text{NO}_3^-$  [23]. The inference is during WM, while primary production doubled in response to nutrient enrichment, regenerated production also remained high due to an active recycling. Thus, much of the nitrate in the euphotic zone that remained unconsumed during WM was conserved for the following SIM for phytoplankton growth [24].
- (2) Time-series measurements in the Arabian Sea ( $21^\circ\text{N}$ ,  $64^\circ\text{E}$ ) during WM showed large mixed layer variations in the dissolved inorganic nitrogen and new production leading to a different food web [25].

- (3) The Arabian Sea surface waters sustain very low chlorophyll *a* during SIM (March–May) following the formation of a warm pool and stratification, which inhibit entrainment of nutrients into the surface [11]. It is therefore likely that the nitrate rich waters of the northern Arabian Sea have entrained southward (Figure 5) stimulating higher surface primary production in the SEAS. Since many of these conditions are highly variable, further observations are required to verify the above views.

The Aqua MODIS (resolution  $4 \times 4$  km) images depict the daily averaged chlorophyll *a* distribution in the SEAS during 6 March to 13 April 2004 (Figure 9). There are patches of productive areas in the coastal waters between  $11^{\circ}\text{N}$  and  $15^{\circ}\text{N}$ , whereas most of the regions remained oligotrophic. For instance, a wave like pattern representing  $>1 \text{ mg m}^{-3}$  chlorophyll *a* can be seen from  $11^{\circ}30'\text{N}$  to the north along the coast. The MODIS chlorophyll peaks ( $>1.5 \text{ mg m}^{-3}$ ) corresponding to the two coastal sites ( $12^{\circ}\text{N}$  and  $13^{\circ}30'\text{N}$  respectively) are well corroborated with the measured values during the present study. This is interesting because the chlorophyll *a* concentrations in the AS south of  $20^{\circ}\text{N}$  during SIM are normally below  $0.25 \text{ mg m}^{-3}$  [18]. Banse [26] has observed that the two bloom periods observed in the north AS (SWM and shortly after NEM) are well separated by a SIM period of low phytoplankton biomass, since the seasonal heating inhibits the nutrient supply from the deep. The increased irradiance coupled with stratification caused by the subducted ASHSW is probably supporting a high chlorophyll *a* biomass (DCM) between 40–80 m (Figure 8) with lower photosynthetic potential (high Chl/C ratio).

### Conclusion

The study has identified some of the biogeochemical features of SEAS during SIM. Normally, the NAS experiences enhanced biological production during winter monsoon, while the SEAS (south of  $13^{\circ}\text{N}$ ) remain oligotrophic. However, there was a high biological production in the SEAS between  $13^{\circ}\text{N}$  and  $15^{\circ}\text{N}$  during SIM, caused by surface stratification and nitrate-rich waters entrained from the NAS. The DCM observed in the offshore waters just below the subducting ASHSW was typical of phytoplankton adapted to light and nutrients.

### Acknowledgements

We thank Dr. S.R. Shetye, Director, National Institute of Oceanography, Goa, Mr. Rasik Ravindra, Director, NCAOR, Goa and the Scientist-in-Charge, NIO Regional Centre, Cochin for the encouragement. We are grateful to all participants of cruise SS 223 of FORV Sagar Sampada for help. This investigation was carried out under the programme “Environment and Productivity Patterns in the Indian EEZ” funded by Centre for Marine Living Resources and Ecology (CMLRE), Ministry of Earth Sciences, Govt. of India, New Delhi. The critical review given by Prof. K. Banse has really helped us to improve the manuscript substantially. This is NCAOR contribution No. 25/2012.

### References

- [1] S.R. Shetye, A.D. Gouveia, S.S.C. Shenoi, G.S. Michael, D. Sunder, A.M. Almedia, and K. Santanam, *The coastal current off western India during the northeast monsoon*, Deep-sea Res. 38 (1991), pp. 1517–1529.

- [2] T. Pankajakshan and A.K. Gosh, *Surface layer temperature inversion in the Arabian Sea during winter*, J. Oceanograph. 48 (1992), pp. 293–304.
- [3] P.N. Vinayachandran and J. Kurian. *Modeling Indian Ocean circulation: Bay of Bengal fresh plume and Arabian Sea mini warm pool*, Proceedings of the 12th Asian Congress of Fluid Mechanics, Daejeon, Korea, 2008.
- [4] P.M. Muraleedharan and S. Prasanna Kumar, *Arabian Sea upwelling – A comparison between coastal and open ocean regions*, Current Sci. 71 (1996), pp. 842–846.
- [5] D.J. Rochford, *Salinity maxima in the upper 100m of the north Indian Ocean*, Australian J. Mar. Freshwater Res. 15 (1964), pp. 1–24.
- [6] D. Shankar, *Seasonal cycle of sea level and currents along the coast of India*, Current Sci. 78 (2000), pp. 279–288.
- [7] K.V. Sanilkumar, P.V. Hareeshkumar, J. Joseph, and J.K. Panigrahi, *Arabian Sea mini warm pool during May 2000*, Current Sci. 86 (2003), pp. 180–184.
- [8] P.N. Vinayachandran, D. Shankar, J. Kurian, F. Durand, and S.S.C. Shenoi, *Arabian Sea mini warm pool and the monsoon onset vortex*, Current Sci. 93 (2007), pp. 203–214.
- [9] J.P. McCreary, P.K. Kundu, and R.L. Molinari, *A numerical investigation of dynamics, thermodynamics and mixed layer process in the Indian Ocean*, Progress in Oceanograph. 31 (1993), pp. 181–244.
- [10] M. Madhupratap, S.P. Kumar, P.M.A. Bhattathiri, M.D. Kumar, S. Raghukumar, K.K.C. Nair, and N. Ramaiah, *Mechanism of the biological response to winter cooling in the northern Arabian Sea*, Nature 384 (1996), pp. 549–552.
- [11] S. Prasannakumar, M. Madhupratap., M. Dileepkumar., M. Gauns, P.M. Muraleedharan, V.S.S.S. Sarma, and S.N. deSouza, *Physical control of primary productivity on a seasonal scale in the central and eastern Arabian sea*, Proceed. Ind. Acad. Sci. (Earth and Planet Sci.). 109 (2001), pp. 411–433.
- [12] J. Marra and R.T. Barber, *Primary productivity in the Arabian Sea: A synthesis of JGOFS data*, Progress Oceanograph. 65 (2005), pp. 159–175.
- [13] S. Nielsen, *The use of radioactive carbon (C14) for measuring organic production in the sea*, J. Cons. Int. Explor. Mer. 18 (1952), pp. 117–140.
- [14] P.M.A. Bhattathiri, A. Pant, S. Sawant, M. Gauns, S.G.P. Matondkar, and R. Mohanraju, *Phytoplankton production and chlorophyll distribution in the eastern and central Arabian Sea in 1994–1995*, Current Sci. 71 (1996), pp. 847–851.
- [15] J.D.H. Strickland and T.R. Parsons, *A Practical Handbook of Sea Water Analysis*, Bull. Fisheries Res. Board, Canada, 1972.
- [16] UNESCO, *Protocols for the Joint Global Ocean Flux Study (JGOFS) core measurements*, Scientific Committee on Oceanic Research. Manuals and Guides, Geneva, 1994.
- [17] H.K. Bathen, *Heat storage and advection in the northern Pacific Ocean*, J. Geophys. Res. 76 (1971), pp. 676–687.
- [18] J.D. Wiggert, R.R. Hood, K. Banse, and J.C. Kindle, *Monsoon-driven biogeochemical processes in the Arabian Sea*, Progress Oceanograph. 65 (2005), pp. 176–213.
- [19] S.S.C. Shenoi, D. Shankar, G.S. Michael, J. Kurian, K.K. Varma, M.R. Rameshkumar, A.M. Almeida, A.S. Unnikrishnan, W. Fernandes, N. Barreto, C. Gnanaseelan, R. Mathew, K.V. Praju, and V. Mahale, *Hydrography and water masses in the southeastern Arabian Sea during March–June 2003*, J. Earth Syst. Sci. 114 (2005), pp. 475–491.
- [20] D. Shankar, P.N. Vinayachandran, and A.S. Unnikrishnan, *The monsoon currents in the north Indian Ocean*, Progress Oceanograph. 52 (2002), pp. 63–120.
- [21] T.G. Prasad, M. Ikeda, and S. Prasannakumar, *Seasonal spreading of the Persian Gulf water mass in the Arabian Sea*, J. Geophys. Res. 106 (2001), pp. 17059–17071.
- [22] N.V. Madhu, R. Jyothibabu, P.A. Maheswaran, K.A. Jayaraj, and C.T. Achuthankutty, *Enhanced chlorophyll a and primary production in the northern Arabian Sea during the spring intermonsoon due to green Noctiluca (N. scintillans) bloom*, Mar Biol Res. 8 (2012), pp. 182–188.

- [23] J.J. McCarthy, C. Garside, and J.L. Nevins, *Nitrogen dynamics during the Arabian Sea northeast monsoon*, *Deep-sea Res.* 46 (1999), pp. 1623–1664.
- [24] R.T. Barber, J. Marra, R.R. Bidigare, I.A. Codispoti, D. Halpern, and Z. Johnson, *Primary productivity and its regulation in the Arabian Sea during 1995*, *Deep-Sea Res.* 48 (2001), pp. 1127–1172.
- [25] S.W.A. Naqvi, V.V.S.S. Sarma, and D.A. Jayakumar, *Carbon cycling in the northern Arabian Sea during the northeast monsoon: Significance of salps*, *Mar. Ecol. Prog. Ser.* 226 (2002), pp. 35–44.
- [26] K. Banse, *Seasonality of phytoplankton chlorophyll in the central and northern Arabian Sea*, *Deep-sea Res.* 34 (1987), pp. 713–723.